

Finite Larmor radius effects on the ($m = 2, n = 1$) cylindrical tearing mode

Y. Chen, J. Chowdhury, S. E. Parker, and W. Wan

Center for Integrated Plasma Studies, University of Colorado at Boulder, Boulder, Colorado 80309, USA

(Received 4 March 2015; accepted 13 April 2015; published online 22 April 2015)

New field solvers are developed in the gyrokinetic code GEM [Chen and Parker, *J. Comput. Phys.* **220**, 839 (2007)] to simulate low- n modes. A novel discretization is developed for the ion polarization term in the gyrokinetic vorticity equation. An eigenmode analysis with finite Larmor radius effects is developed to study the linear resistive tearing mode. The mode growth rate is shown to scale with resistivity as $\gamma \sim \eta^{1/3}$, the same as the semi-collisional regime in previous kinetic treatments [Drake and Lee, *Phys. Fluids* **20**, 1341 (1977)]. Tearing mode simulations with gyrokinetic ions are verified with the eigenmode calculation. © 2015 AIP Publishing LLC.
[\[http://dx.doi.org/10.1063/1.4919023\]](http://dx.doi.org/10.1063/1.4919023)

I. INTRODUCTION

Gyrokinetic simulation has been used to study the tearing mode by many authors.^{1–4} It was first applied to small-scale collisionless tearing mode⁵ by Sydora,¹ and more recently applied to the low- n (n is the toroidal mode number) magnetohydrodynamic (MHD) scale tearing modes in tokamaks.⁶ Both the ion kinetic effects and the electron kinetic effects are of great interest. Ion kinetic effects are found to be unimportant in slab geometry,^{2,5} but can be important in toroidal geometry, as found for energetic particles.⁷ In plasmas with a weak guide field, the gyrokinetic model for ions may be inadequate and a full Lorentz ion model is needed.⁸ Gyrokinetic simulations have been used to study electron kinetic effects near the tearing layer such as electron Landau damping, collisions, as well as electron finite-Larmor-radius (FLR) effects.^{1–3} Simulations with the astroGK code⁹ highlights the lack of appropriate approximate closure scheme between the perturbed electron pressure and density that is needed in fluid models.¹⁰ Within the scope of the gyrokinetic simulations, kinetic electron effects are the more difficult to include, especially in the long wavelength limit. The perturbative approach based on the small parameter $\omega/k_{\parallel}v_{te} \ll 1$ (Ref. 11) breaks down for the tearing mode in the tearing layer, and requires special extension for the tearing mode.¹² Due to the so-called “Cancellation Problem,”¹³ low- n MHD scale modes in present day tokamaks are in general very challenging in gyrokinetic simulation with fully kinetic electrons.¹⁴ The difficulty is exacerbated for low- n tearing modes due to their smaller growth rates.

This work represents our first effort to extend the Particle-in-Cell (PIC) code GEM¹⁵ to the study of low- n tearing modes in tokamaks. GEM is originally developed for the simulation of drift wave turbulence. For high- n drift waves, an approximation is made in the Laplacian ∇_{\perp}^2 operator that appears in the Ampere’s equation, namely, only derivatives of the second order in the perpendicular plane (the $x - y$ plane in the field-aligned coordinates) are retained in the operator. In slab geometry, only the second derivatives are involved, but in more general geometry (cylindrical or toroidal) first order derivatives are involved and not negligible. For the Alfvén eigenmodes, a direct comparison

between the approximate and the exact operator indicates that the high- n approximation can be valid for $n = 2$.¹⁶ However, we have not been able to observe the $n = 1$ tearing mode using the same code, indicating a breakdown of the high- n approximation for $n = 1$. Our first step in extending the code to include the $n = 1$ mode is to develop the field solvers (i.e., solvers for the gyrokinetic Poisson equation and the parallel Ampere’s equation) that avoid any high- n approximation and to do this in the gyrokinetic ion/fluid electron hybrid model.¹⁷ The field equations are now solved in the (r, θ) -plane, instead of the (x, y) -plane in the field-aligned coordinates. Since particle positions are still evolved in the field-aligned coordinates, a mapping between the toroidal coordinates (r, θ, ζ) and the field-aligned coordinates (x, y, z) are needed and constructed. Because of the low growth rates of low- n tearing modes, numerical dissipation must be minimized. For simplicity, here we restrict to cylindrical geometry, for which an eigenmode analysis of the zero- β fluid equations can be readily developed and used as a verification for the simulation.

In the process of verifying GEM for low- n capability, we find new results on the growth rate scaling with resistivity for the resistive tearing mode. It is long recognized that the width of the tearing layer of the resistive tearing mode in present day tokamaks is much smaller than the ion Larmor radius,¹⁸ hence, the FLR corrections to the ion polarization density in the vorticity equation must be retained. The classical tearing mode theory¹⁹ assumes the tearing layer width exceeds the ion Larmor radius and predicts that the mode growth rate scales with resistivity as $\gamma \sim \eta^{0.6}$ at sufficiently low η . In this paper, we develop an eigenmode analysis that is based on the model equations with the full gyrokinetic form of the ion polarization density, and obtain a scaling of $\gamma \sim \eta^{1/3}$ in the low η regime. This scaling agrees with the kinetic theory of Drake and Lee⁵ for the semi-collisional regime. It turns out that, for the cylindrical geometry considered, the FLR effect on the ion polarization density is the dominant ion kinetic effect. Other ion kinetic effects remain small, as predicted by theory and verified in initial value simulations.

This paper is organized as follows. Section II describes the simulation model. Section III discusses the validity of the

approximations usually made in simulation of high- n modes, and presents a new discretization procedure for the field equations. Section IV presents eigenmode analysis of the reduced-MHD equation with FLR correction. Initial value simulation results are presented in Sec. V, and summary in Sec. VI.

II. MODEL EQUATIONS

We consider a cylindrical equilibrium with a circular cross section. The equilibrium magnetic field is $\mathbf{B} = B_Z(r)\hat{\mathbf{Z}} + B_\theta(r)\hat{\boldsymbol{\theta}}$, with (r, θ, Z) being the usual right-handed cylindrical coordinates. Considered as an approximation to a large-aspect ratio tokamak with major radius R_0 and the safety factor profile $q(r)$, Z is related to the toroidal angle ζ through $Z = R_0\zeta$, and $q(r) = B_Z r / B_\theta R_0$. The equilibrium force balance $-\nabla p + \mathbf{J} \times \mathbf{B} = 0$ yields

$$\frac{1}{2} \frac{d}{dr} B^2 = -\mu_0 p'(r) - B_\theta^2 / r, \quad (1)$$

which relates the guiding center drift (proportional to ∇B) to the pressure profile $p(r)$. Here μ_0 is the vacuum permittivity.

In this paper, we use the gyrokinetic ion/fluid electron hybrid model^{17,20} to study the $(m, n) = (2, 1)$ resistive tearing mode in cylindrical plasmas. Details of the hybrid model can be found in Chen and Parker²⁰ and Chen *et al.*¹⁷ A brief summary is given here. The field perturbations are given by $\mathbf{E} = -\nabla\phi - (\partial A_\parallel / \partial t)\mathbf{b}$ and $\delta\mathbf{B}_\perp = \nabla A_\parallel \times \mathbf{b}$, with \mathbf{b} being the unit vector along the equilibrium magnetic field. The parallel magnetic field perturbation is neglected. The fluid electron model consists of the electron continuity equation and the isothermal condition for the electron temperature perturbation. The vorticity equation, or the time derivative of the gyrokinetic Poisson equation, is used to obtain ϕ .¹⁷ The potential A_\parallel is obtained by time evolving $\partial A_\parallel / \partial t = -\nabla_\parallel \phi - E_\parallel$. The parallel electric field E_\parallel is determined by the Ohm's equation. The ions are described by the gyrokinetic equation, solved with the δf PIC method. In this paper, we consider only the resistive tearing mode, and the generalized Ohm's law simplifies to

$$E_\parallel = \eta j_\parallel, \quad (2)$$

where η is the resistivity and j_\parallel is the perturbed electric current. The vorticity equation is

$$-\dot{n}_p = \frac{1}{\beta_u} \nabla_\parallel \nabla_\perp^2 A_\parallel + \delta\mathbf{B}_\perp \cdot \nabla \nabla (n_0 U_{\parallel 0}) + \frac{1}{m_e \Omega_e B^2} \mathbf{B} \times \nabla \mathbf{B} \cdot \nabla (\delta P_\perp + \delta P_\parallel) + \dot{\delta n}_i, \quad (3)$$

where n_p is the ion polarization density. The closure relation for the perturbed electron pressure is $\delta P_\perp = \delta P_\parallel = n_0 \delta T_e + T_e \delta n_e$, and δT_e is given by the isothermal condition along the perturbed field line.¹⁷ By combining the Ohm's law with the Ampere's equation $-\nabla^2 A_\parallel = \beta_u j_\parallel$, the evolution equation for A_\parallel becomes

$$\frac{\partial A_\parallel}{\partial t} = -\nabla_\parallel \phi + \frac{\eta}{\beta_u} \nabla_\perp^2 A_\parallel. \quad (4)$$

Equations (3) and (4) are written in dimensionless form. Here, $\beta_u \equiv \mu_0 n_u T_u / B_u^2$, B_u is the unit for magnetic field, usually chosen to be the on-axis toroidal field, n_u is a normalization unit for density, and T_u is the unit for temperature. The unit for time is $t_u = m_p / e B_u$ with m_p being the proton mass, the unit for velocity is $v_u = \sqrt{T_u / m_p}$, and the unit for length is $x_u = m_p v_u / e B_u$. In Eq. (3), $n_0(r)$ is the equilibrium electron density, $U_{\parallel 0}(r)$ is the equilibrium electron flow velocity, and $\dot{\delta n}_i$ is the rate of change of the perturbed ion density. The electron flow velocity $U_{\parallel 0}$ is computed from the equilibrium magnetic field using the Ampere's law, assuming the equilibrium current is all carried by electrons. We consider a plasma of a single charged ion species with mass m_i . The ion polarization density n_p (Ref. 21) used in this paper is given by

$$n_p(r) = -\frac{n_i(r)}{T_i(r)} \sum_{k_\perp} (1 - \Gamma_0(b)) \phi_{k_\perp} e^{i k_\perp \cdot \mathbf{x}}, \quad (5)$$

where Γ_0 is the Γ -function, $b = k_\perp^2 v_{Ti}^2 / \Omega_i^2$ and $v_{Ti} = \sqrt{T_i / m_i}$ is the ion thermal speed. A more general form of the polarization density is the integral form.²¹ The form, Eq. (5), is derived from the general form by assuming the ion density and temperature to be locally flat. Part of the profile effects are captured in Eq. (5) through the explicit dependence of n_i and T_i (v_{Ti}) on r . This form of n_p is adequate for the tearing modes studied here because ϕ is important only near the tearing layer and varies much more rapidly in r than the equilibrium density and temperature. In Eq. (5), the potential is to be understood as decomposed into Fourier modes in the Cartesian plane locally perpendicular to the equilibrium magnetic field. In slab geometry, this spectral form can be used directly for a spectral solution of the gyrokinetic Poisson equation.^{3,9} In a more general geometry, the spectral approach is more subtle, as explained in the next Section.

We note that the field A_\parallel is usually denoted by Ψ in the literature on the tearing mode. Equations (3) and (4) are identical to the model equations studied by Furukawa *et al.*²² when n_p is taken to be the MHD limit (see below) and the plasma pressure effects are neglected.

The Laplacian operator ∇_\perp^2 should be interpreted as the Laplacian in the plane locally perpendicular to the equilibrium magnetic field, which is not the (r, θ) plane.²³ However, following the previous studies of tearing modes in cylindrical plasmas^{18,22} and consistent with the reduced-MHD ordering,²⁴ we will interpret the Laplacian operator ∇_\perp^2 as the Laplacian operator in the (r, θ) -plane, i.e., for arbitrary f

$$\nabla_\perp^2 f = \frac{\partial^2 f}{\partial r^2} + \frac{1}{r^2} \frac{\partial^2 f}{\partial \theta^2} + \frac{1}{r} \frac{\partial f}{\partial r}. \quad (6)$$

III. A NOVEL DISCRETIZATION PROCEDURE FOR THE ION POLARIZATION OPERATOR

A. Breakdown of the high- n approximation

The Laplacian operator, Eq. (6), differs from the previous form used in GEM and other high- n micro-turbulence codes,^{25,26} which is a differential operator in the (x, y) -plane of the field-aligned coordinates,^{15,26} valid for high- n

perturbations. It is instructive to examine this operator and see just where the high- n approximations break down. Define the field-line-following coordinates as

$$x = r - r_0, \quad (7)$$

$$y = \frac{r_0}{q_0} \left(\int_0^\theta \hat{q} d\theta - \zeta \right), \quad (8)$$

$$z = q_0 R_{\Psi_0} \theta, \quad (9)$$

with R_{Ψ_0} being an arbitrary constant, usually chosen to be the major radius of the magnetic axis. To a good approximation, $\nabla_\perp^2 \approx \nabla^2$, which is expressed in the field-aligned coordinates as

$$\begin{aligned} \nabla_\perp^2 \phi &= \frac{\partial^2 \phi}{\partial x^2} |\nabla x|^2 + 2 \frac{\partial^2 \phi}{\partial x \partial y} \nabla x \cdot \nabla y + \frac{\partial^2 \phi}{\partial y^2} |\nabla y|^2 \\ &+ \frac{\partial \phi}{\partial x} \nabla \cdot \nabla x + \frac{\partial \phi}{\partial y} \nabla \cdot \nabla y \\ &+ \frac{\partial^2 \phi}{\partial x \partial z} \nabla x \cdot \nabla z + \frac{\partial^2 \phi}{\partial y \partial z} \nabla y \cdot \nabla z \\ &+ \nabla \cdot \left(\frac{\partial \phi}{\partial z} \nabla z \right). \end{aligned} \quad (10)$$

For high- n modes only terms in the first line are retained, so that the field equation is quasi-two-dimensional. This reduction in dimension is a main advantage of the high- n approximation. For $n=1$, $m \sim 1$, this is a poor approximation. The last term cannot be neglected

$$\nabla \cdot \left(\frac{\partial \phi}{\partial z} \nabla z \right) = \dots + \frac{\partial^2 \phi}{\partial z^2} |\nabla z|^2 \sim \dots + \frac{\phi}{r^2}, \quad (11)$$

which competes with $\frac{\partial^2 \phi}{\partial y^2} |\nabla y|^2 \sim \frac{m^2}{r^2} \phi$ for $m \sim 1$. Another high- n approximation hides in the kink term in the vorticity equation

$$\delta \mathbf{B}_\perp \cdot \nabla (n_0 u_{\parallel 0} / B) = \left(\frac{q r_0}{q_0 r} \frac{\partial A_\parallel}{\partial y} + \frac{q_0 R_0}{r} \frac{\partial A_\parallel}{\partial z} \right) \frac{d}{dr} (n_0 u_{\parallel 0} / B). \quad (12)$$

The term proportional to $\partial A_\parallel / \partial z$ must be retained for $m \sim 1$.

This observation pertains to other codes that utilize the high- n flux-tube model.^{15,25,26} The exact toroidal mode number for which the high- n approximation breaks down can vary for different problems. In some case, it remains valid for the $n=2$ Toroidal Alfvén Eigenmode.¹⁶ Notice that one of the important omitted term, Eq. (11), involves derivatives in z . This term makes the Laplacian operator three-dimensional, and discretization of the field equation in the field-aligned coordinates is no longer advantageous. Rather than adding the missing terms in Eq. (10) in the existing field solvers, we choose to develop new field solvers for low- n simulations that are directly based on Eq. (6).

B. Discretization of the ion polarization

In an axisymmetric tokamak there is no coupling among toroidal modes in the linear regime, hence field solving

should be decomposed in the toroidal direction. The situation is more complicated in the poloidal direction. In the high- n case, there is likely a large number of poloidal harmonics across the radius that need to be retained for an adequate representation of a single n , but centered around $m = nq(r)$ at each radius for flute-like modes ($k_\parallel \approx 0$). A large number of m 's need be resolved if Fourier decomposition is used in the poloidal direction. On the other hand, if the field-aligned coordinates are used, a relatively small number of grids in the z -direction, independent of r , is sufficient. Thus for high- n drift waves, solving the field equations in the field-aligned coordinates is a natural choice. For low- n modes, the reverse holds. One expects only a small number of poloidal harmonics are significant for $n=1$, even if there is poloidal coupling. In the cylindrical geometry, there is no poloidal coupling. These considerations strongly suggest a spectral approach in the poloidal angle in solving the field equations for low- n modes. This means only the radial dimension is discretized with a set of grid points $\{r_i = r_{\text{in}} + i\Delta r : i = 0, 1, 2, \dots, N_r\}$ ($\Delta r = (r_{\text{out}} - r_{\text{in}}) / N_r$, r_{in} and r_{out} are the inner and outer boundary of the simulation domain, respectively). Assume the electric potential for a given toroidal mode number n is represented as

$$\phi(r_i, \theta, \zeta) = \sum_m \phi_{nm}(r_i) e^{im\zeta + im\theta}, \quad (13)$$

with $\iota = \sqrt{-1}$. We then look for a discretization of n_p such that the discretized ion polarization density is given by

$$n_p(r_i, \theta, \zeta) = \sum_m \left(\sum_{m'} \sum_j M_{mm'}(i, j) \phi_{nm'}(r_j) \right) e^{im\zeta + im\theta}, \quad (14)$$

which allows for poloidal coupling. Here $M_{mm'}(i, j)$ is a $(N_r - 1) \times (N_r - 1)$ matrix. The boundary conditions $\phi(r_{\text{in}}) = \phi(r_{\text{out}}) = 0$ is applied so the number of unknowns for each m is $N_r - 1$. This boundary condition is appropriate for any $m=2$ MHD modes (only $m=2$ modes are considered in this paper), as long as the inner boundary r_{in} is reasonably small, say, $r_{\text{in}}/a < 0.1$. For the tearing modes, the boundary condition can be used for larger values of r_{in} because of the peculiar ϕ mode structures (see the next Section). This discretization is different from the scheme of Mishchenko *et al.*²⁷ which is based on the integral form of the polarization density evaluated using a Monte-Carlo method, and different from that of Nishimura *et al.*²⁸ which employs the Pade approximation and uses a set of two-dimensional (2D) finite elements to represent ϕ . In the case of low- n modes with few coupled poloidal harmonics, the number of unknowns in this spectral approach is significantly smaller than the number of 2D finite elements needed to resolve the poloidal mode structure. This is important for numerical efficiency, especially for the tearing mode since a large number of radial grid points are needed to resolve the thin tearing layer.

The matrix M is constructed by first constructing an auxiliary matrix M' that is an accurate discretization of the polarization density in the Cartesian plane perpendicular to the local magnetic field, according to the general expression (Eq. (5)). The matrix M is then obtained by expressing ϕ at

each Cartesian grid in the local perpendicular plane in terms of the spectral representation (Eq. (13)). Details of this procedure is given in the Appendix. Fig. 1 compares the accuracy of the discrete ion polarization density for different number of grids in the local $x - y$ -plane (see the Appendix) and compares the discrete form with the Pade approximation. Over a large range of the wave number, $0.01 < k_{\perp}\rho_i < 10$, the relative discretization error is less than 1%, a significant improvement over the Pade approximation.

IV. EIGENMODE ANALYSIS WITH FINITE-LARMOR-RADIUS EFFECT

In this section, we develop an eigenmode analysis for Eqs. (3) and (4) neglecting the ion contribution and the electron pressure contribution in the vorticity equation. Assuming perturbation of the form $\sim \exp(-i\omega t + im\theta + in_z z)$, then $\nabla_{\parallel} = i(n + m/q)/R_0$. Using the finite difference for the radial derivatives, the dispersion relation can be cast into the form

$$\det(A - \omega B) = \det(B) \cdot \det(AB^{-1} - \omega I) = 0, \quad (15)$$

where A and B are two $2(N_r - 1) \times 2(N_r - 1)$ matrices. This dispersion relation is of the form of a standard matrix eigenvalue problem and can be readily solved using the LAPACK software library.

We consider a cylindrical equilibrium with the safety factor profile $q(r) = 1.5(1 + (r/a)^2)$, a constant density profile and a temperature profile $T_i(r) = T_e(r) \sim 1 - (r/a)^2$, with an on-axis plasma beta of $\beta(0) \equiv 4\mu_0 n_0 T_i(0)/B^2 = 0.004$. The ion has charge $q = |e|$ and mass $m_i/m_p = 2.5$. The size of the plasma is $a/\rho_i = 740$, where ρ_i is the main ion gyro-radius at the axis. The aspect ratio is $R_0/a = 4$. The q -profile and the equilibrium electron flow profile are plotted in Fig. 2. We

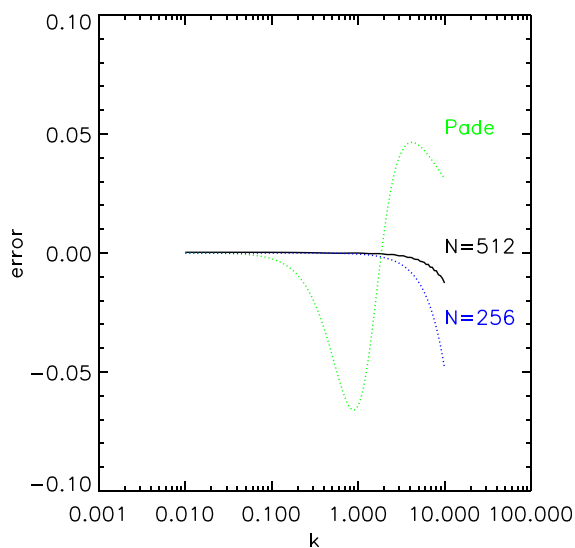


FIG. 1. Relative error of the discrete ion polarization vs. the perpendicular wavenumber. The relative error is defined to be $(n_{\text{disc}} - n_{\text{exac}})/n_{\text{exac}}$, for example, where $n_{\text{exac}} = 1 - \Gamma_0(b)$ is the exact result, and n_{disc} is the result of applying the new discretization procedure to the single Fourier mode. N is the number of grids in the local perpendicular plane in Eq. (A2). The error for the Pade approximation is also shown. $N = 256$ is used in simulations.

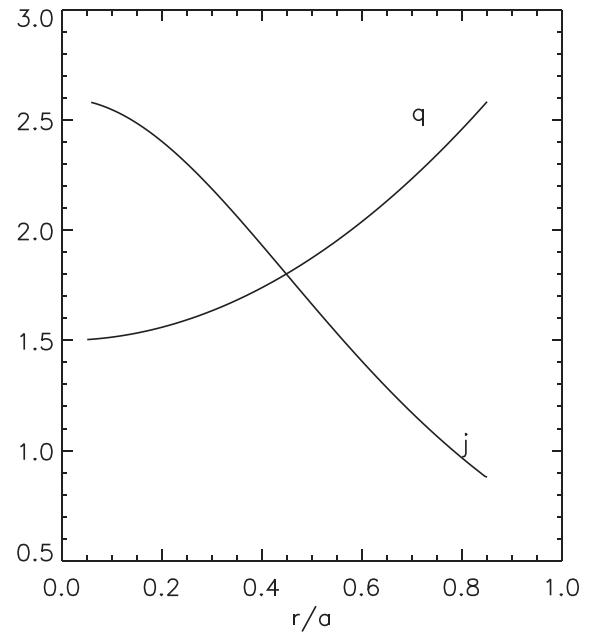


FIG. 2. Safety factor and current profiles.

study the $(m, n) = (2, -1)$ tearing mode which has a tearing layer located near the $q = 2$ surface at $r/a = 0.577$.

The growth rate of the mode versus resistivity is shown in red in Fig. 3. The radial domain is $0.05 \leq r/a \leq 1$, and the number of uniformly spaced radial grids is $N_r = 2048$. The results obtained with the MHD approximation for the ion polarization density is also shown in black, with the theoretical scaling of $\gamma \sim \eta^{0.6}$ shown in green. At large resistivity, $\eta > 10^{-6}$, the two results agree very well, as is expected because the tearing layer width is large and FLR effects on the ion polarization density are small. At smaller resistivity, the two results do not agree, and FLR effects appear to

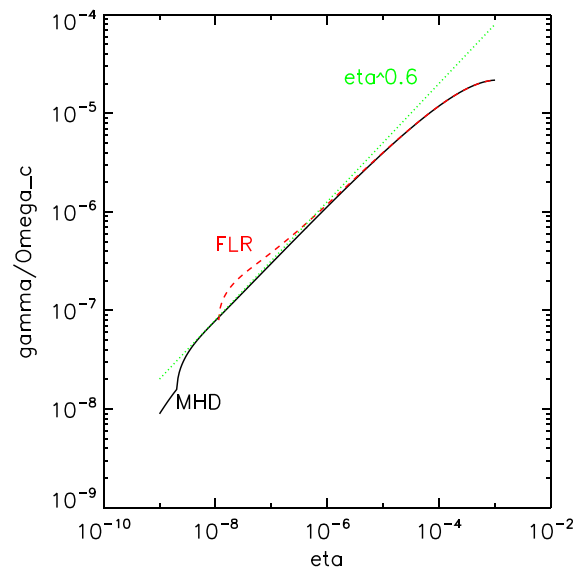


FIG. 3. Tearing mode growth rate vs. resistivity obtained from eigenmode analysis with a radial domain of $\Delta r/a = 0.95$. The dashed line (red) is obtained with the FLR effect. The solid line is obtained with the MHD vorticity equation, obeys the classical scaling $\sim \eta^{0.6}$ as indicated by the dotted (green) line. At low resistivity, both eigenmode results deviate from a power scaling due to poor resolution.

increase the mode growth rate significantly. However, as resistivity decreases further, both results display unexpected behaviour. At very small resistivity, $\eta < 10^{-8}$, the MHD result deviates from the theoretical scaling. These behaviours indicate that the mode structure is under-resolved as the tearing layer becomes narrower. It is computationally prohibitive to increase N_r further. A natural approach is to use non-uniform radial grids, using more grids per unit length in the tearing layer. Here we take another approach, which is to reduce the size of the eigenmode problem domain, using the appropriate “outer” boundary condition. Fig. 4 shows the mode structure for $\eta = 1.2 \times 10^{-8}$. The tearing mode is characterized by a broad structure for the vector potential, but a very narrow structure for the electric potential. As resistivity decreases the broad mode structure of A_{\parallel} away from the resonance layer does not change and is determined by the external MHD equations. The eigenmode problem can be solved on a radial domain that is much smaller than the minor radius, as long as the correct outer boundary conditions are used for A_{\parallel} . The boundary conditions for ϕ remain the same, i.e., $\phi = 0$ at the outer boundaries. The appropriate boundary condition for A_{\parallel} takes the form

$$\begin{aligned} \left. \frac{dA_{\parallel}}{dr} \right|_{r_{in}} &= a_- A_{\parallel}(r_{in}), \\ \left. \frac{dA_{\parallel}}{dr} \right|_{r_{out}} &= a_+ A_{\parallel}(r_{out}). \end{aligned} \tag{16}$$

The coefficients a_- and a_+ are estimated from the eigenmodes using a large radial domain at a small η for which the mode is adequately resolved.

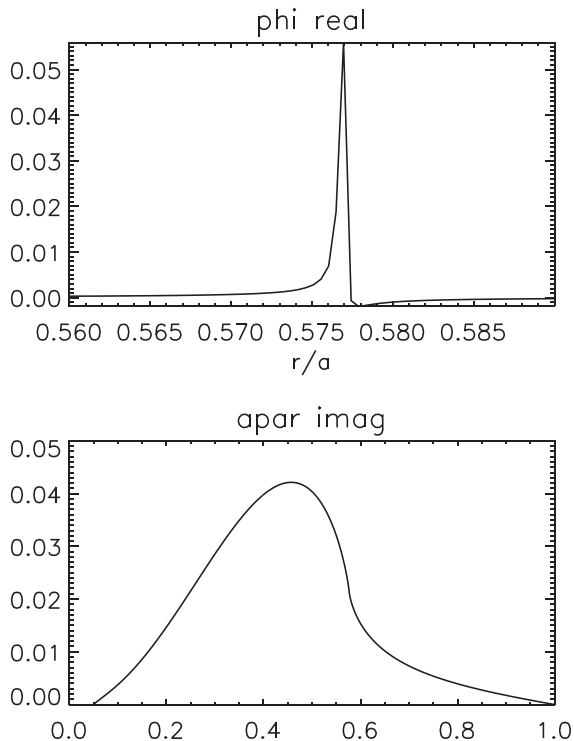


FIG. 4. The tearing eigenmode structure for $\eta = 1.2 \times 10^{-8}$. The electric potential peaks in a narrow region near the tearing layer, but the vector potential has a broad profile.

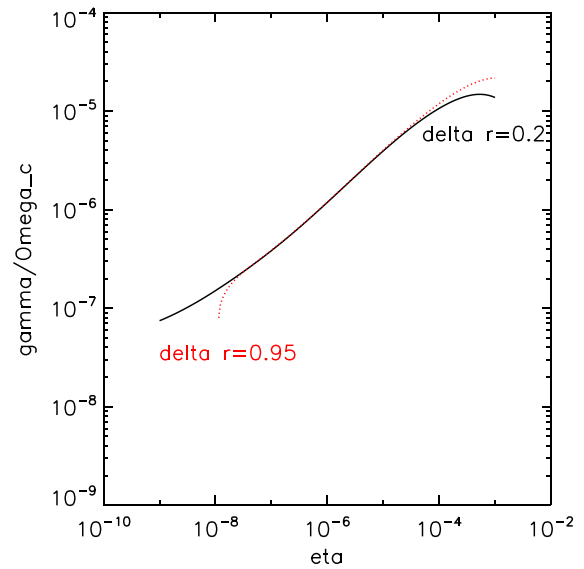


FIG. 5. Comparison between the mode growth rate obtained with $\Delta r/a = 0.2$ (solid) with that obtained with $\Delta r/a = 0.95$ (dashed). The dashed line is the same as the result in Fig. 3 labeled “FLR.” The two results agree for all intermediate values of resistivity. The disagreement at high resistivity is due to the broad tearing layer width, which is affected by the fixed boundary condition for ϕ when $\Delta r/a = 0.2$ is used. However, the validity of the $\Delta r/a = 0.2$ result extends to much lower resistivity due to improved resolution.

Fig. 5 shows the results obtained with a radial domain of $0.477 < r/a < 0.677$, centered around the tearing layer at $r/a = 0.577$. For this domain, all the eigenmodes of Fig. 3 with $\eta < 10^{-5}$ give the same estimated boundary coefficients, and we have checked to ensure that the results of Fig. 5 agree with that of Fig. 3 for all the intermediate values of resistivity. Fig. 6 shows the eigenvalues obtained with $0.477 < r/a < 0.677$ for both MHD and including FLR effects. The validity of these results extends to much lower resistivity, as can be seen by comparing the result of $N_r = 2048$ and the

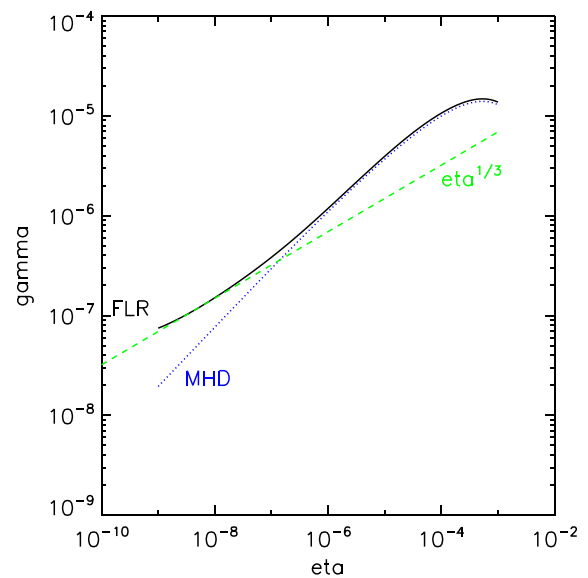


FIG. 6. Compare the semi-collisional scaling with the resistive MHD scaling. Both the resistive MHD results (dotted blue) and the result with FLR effect (solid black) are obtained with $\Delta r/a = 0.2$. The resistive MHD result obeys the scaling $\gamma \sim \eta^{0.6}$ for $\eta \sim 10^{-9}$. The FLR result obeys the scaling $\gamma \sim \eta^{1/3}$ near $\eta \sim 10^{-8}$, in agreement with asymptotic matching analysis.

result of $N_r = 1024$ (not shown). The two results agree for $\eta > 10^{-8}$, indicating the resolution of $N_r = 2048$ on this smaller domain is adequate for $\eta \geq 5 \times 10^{-9}$. The corresponding results with the MHD approximation (blue) is well converged in N_r for all $\eta > 10^{-9}$, and the theoretical scaling of $\gamma \sim \eta^{0.6}$ is clearly seen. If we fit the FLR results near $\eta = 10^{-8}$ with a power law, a scaling of $\gamma \sim \eta^{1/3}$ is obtained as indicated in Fig. 6. This is a much weaker scaling with resistivity than the resistive-MHD result. We have applied the eigenmode analysis to equilibria with different plasma beta and size, and obtained similar weak scaling at low resistivity.

The scaling $\gamma \sim \eta^{1/3}$ can be readily derived in the present fluid electron model. When the tearing layer width is much smaller than the ion Larmor radius, the ion response becomes adiabatic, $n_p = -n_i q_i \phi / T$. Keeping only the first term on the RHS of Eq. (3), the vorticity equation gives

$$\frac{n_i}{T} q_i \gamma \phi = \frac{1}{\beta_i} \nabla_{\parallel} \nabla_{\perp}^2 A_{\parallel}, \quad (17)$$

which can be used to eliminate ϕ in Eq. (4). Define $x = r - r_0$. In the tearing layer, $\nabla_{\perp}^2 \approx d^2/dx^2$, $\nabla_{\parallel}^2 \approx -(mq'x/q_0 R_0)^2$, after eliminating ϕ Eq. (4) then becomes

$$\left(\frac{\eta}{\beta_i \gamma} + \frac{T m^2 q l^2 x^2}{n_i q_i \beta_i \gamma^2 q_0^2 R_0^2} \right) A_{\parallel}''(x) = A_{\parallel}. \quad (18)$$

This equation can be integrated across the tearing layer under the constant A_{\parallel} -approximation¹⁹ to obtain the discontinuity Δ' , the jump in $A_{\parallel}'(x)/A_{\parallel}$ across the tearing layer. The following dispersion relation is then obtained:

$$\gamma = \pi^{-2/3} (a \Delta')^{2/3} \tau_R^{-1/3} \tau_A^{-2/3} (\rho_i / R_0)^{2/3} (n q l a / q_0)^{2/3}, \quad (19)$$

with the resistive time $\tau_R = \mu_0 a^2 / \eta$ and the Alfvén time $\tau_A^2 = a^2 / \mu_0 m_i n_i B^2$. The scaling $\gamma \sim \eta^{1/3}$ is contained in the scaling with τ_R . The tearing layer width Δ is also obtained

$$\Delta / a = \pi^{-1/3} (\Delta' a)^{1/3} (\tau_A / \tau_R)^{2/3} (\rho_i / R_0)^{-2/3} (n q l a / q_0)^{-2/3}. \quad (20)$$

Thus, the tearing mode width scales with resistivity as $\Delta \sim \eta^{2/3}$. Both the mode growth rate scaling and the tearing layer width scaling are identical to that of the semi-collisional regime of Drake and Lee.⁵ It should be noted that, despite the similarity in this scaling, the two cases are quite different in detail. Drake and Lee treats the electrons kinetically, hence their results depend on the electron thermal speed, and the ion response is found to be unimportant. In the present model, the electrons are much simplified, the electron temperature does not appear in the dispersion relation, and the ion adiabatic response is important in deriving the scaling law. Among the three regimes of the tearing modes, the semi-collisional regime is the most relevant for tokamak plasmas,⁵ and a kinetic model for electrons is necessary. Nevertheless, it is interesting to observe that the scaling behaviour of the regime can be obtained by a simple modification in the reduced-MHD model.

V. INITIAL VALUE SIMULATION WITH GYROKINETIC IONS

The new discretization of the polarization density of Section III has also been used in the initial value, δf -PIC code GEM. Both the Ampère's equation and the vorticity equation are now solved Fourier spectrally for each poloidal Fourier component. All time integration, including evolving the particle coordinates and particle weights, and evolving ϕ and A_{\parallel} , are still done in the usual field-aligned coordinates. To minimize numerical dissipation, no digital filtering is applied to (ϕ, A_{\parallel}) . There is another high- n approximation that must be corrected, namely, the kink term is the vorticity equation, the second term on the RHS of Eq. (3). Expressed in the field aligned coordinates, it is

$$\delta \mathbf{B}_{\perp} \cdot \nabla (n_0 U_{\parallel 0}) = \left[\frac{r_0 q}{r q_0} \frac{\partial A_{\parallel}}{\partial y} + \frac{q_0 R_0}{r} \frac{\partial A_{\parallel}}{\partial z} \right] U'_{\parallel 0}(r). \quad (21)$$

For high- n modes, the second term in the bracket is neglected, but it is important to keep this term for $n = 1$.

We continue to use the simplest Ohm's law (Eq. (2)). Thus the electron inertia effect and the electron pressure contribution to E_{\parallel} is neglected. The electron pressure also appears in the vorticity equation, which is included in the simulation. As pointed out by Numato *et al.*,¹⁰ when the electron kinetic effects are important in the tearing layer, there is no simple closure relation suitable for a fluid model. Hence we do not focus on the electron dynamics in this paper. We are currently exploring the kinetic electron effects on the low- n tearing modes using the direct method for electrons,^{13,15} and will report the results in the future. In this paper, we mainly use the resistive tearing mode as a verification for the low- n extension of the code, and briefly address the kinetic ion effects.

We first neglect the kinetic ions and use the simulation as an initial value approach to be compared with the eigenmode

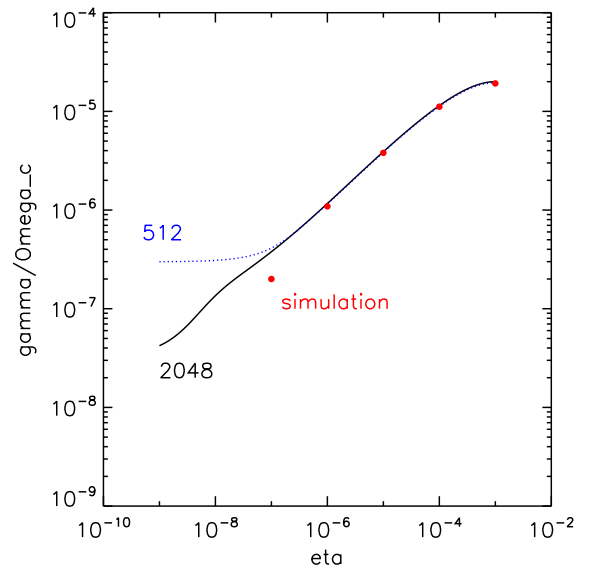


FIG. 7. Compare the growth rate from initial value simulation (round solid data points) with the eigenmode analyses (dotted line with 512 grid points, solid line with 2048 grid points). Both simulation and eigenmode calculation use a radial domain of $\Delta r/a = 0.8$. Simulation uses 512 radial grids.

analysis. For the same equilibrium as in Sec. V, the results are shown in Fig. 7. Both the eigenvalues and the simulation results are obtained with a radial domain of $0.05 < r/a < 0.85$ and $N_r = 512$. Good agreement is obtained for all resistivity values except for $\eta = 10^{-7}$, for which the resolution is insufficient. The mode structures are compared in Fig. 8 for $\eta = 10^{-5}$. These comparisons verify the numerical schemes in the initial value calculation, in particular, the time integration scheme in the field-aligned coordinates, and the numerical mapping between the (x, y, z) -coordinates and the (r, θ, ζ) -coordinates used to bridge the field-solving and time integration.

We now include the electron pressure term and the ion term on the RHS of Eq. (3), separately. Each increases the mode growth rate moderately, as shown in Table I.

VI. SUMMARY AND DISCUSSION

We have implemented new field solvers in GEM for low- n modes, which avoids the high- n approximations of the previous solvers in the field-line-following coordinates. A

new procedure of discretizing the ion polarization term is developed for a mixed finite-difference/spectral method for the gyrokinetic Poisson equation and the gyrokinetic vorticity equation. An eigenmode analysis of the cylindrical resistive tearing mode is used to study the finite-Larmor-radius effect and verify the simulation. The $(m, n) = (2, 1)$ global tearing mode is observed in initial value simulations, in good agreement with eigenvalue calculations. The FLR effect on the ion polarization is found to change the growth rate scaling of the classical resistive tearing mode from $\gamma \sim \eta^{0.6}$ to the semi-collisional scaling of $\gamma \sim \eta^{1/3}$.

The eigenvalue analysis of Sec. IV on a small radial domain is reminiscent of the generalized asymptotic matching method of Furukawa *et al.*²² A small but finite-sized region near the tearing layer is solved with high resolution, with a boundary condition that is determined by solutions in the external region. In this paper, we use the same physical model for the entire plasma, namely, gyrokinetic ion/fluid electron hybrid model. In the fluid limit we are able to demonstrate the equivalence of the eigenmode problem on the reduced radial domain and the original problem on a much

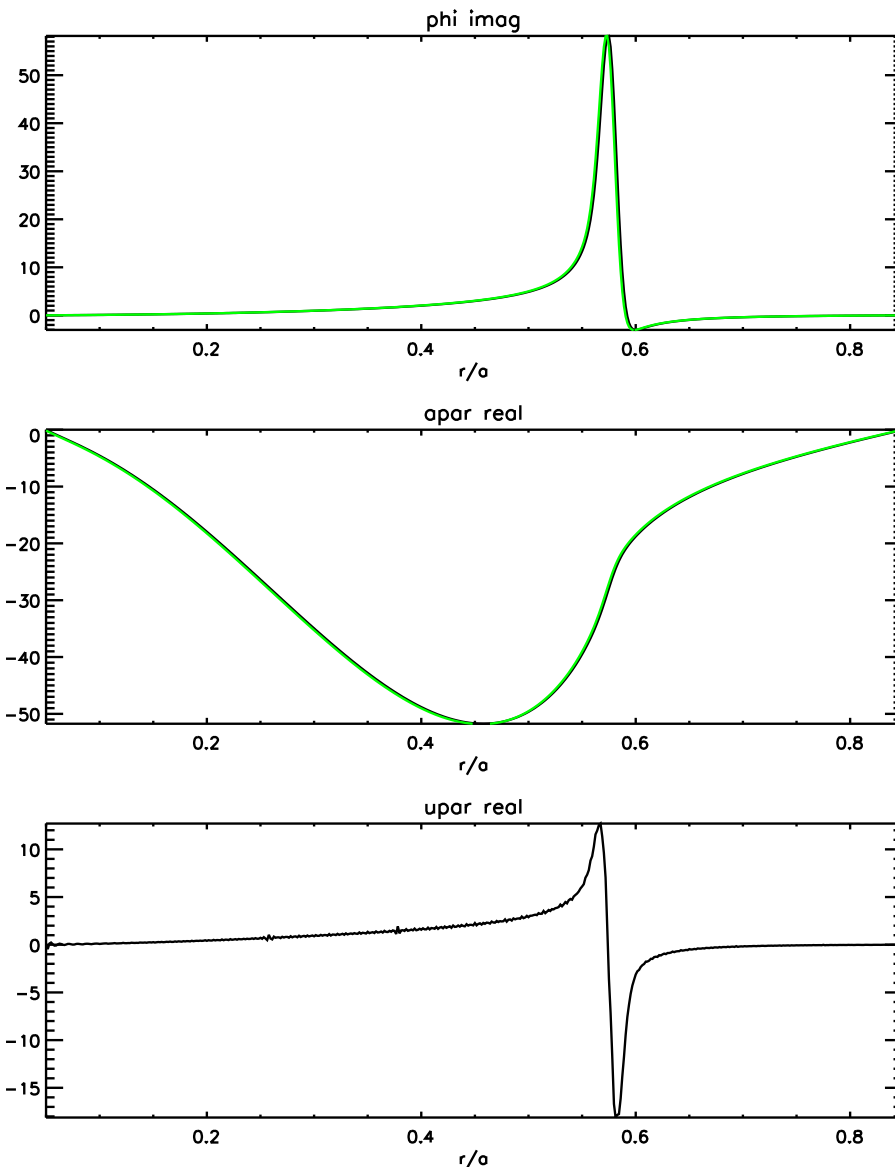


FIG. 8. Compare the mode structure from initial value simulation with the eigenmode result. The mode structures for ϕ (top panel) and for A_{\parallel} (middle panel) agree very well. The lower panel is for the perturbed electron parallel flow from simulation. The resistivity is $\eta = 10^{-5}$.

TABLE I. Electron pressure and kinetic ion effects on tearing mode growth rates.

	$\eta = 10^{-6}$	$\eta = 10^{-5}$	$\eta = 10^{-4}$	$\eta = 10^{-3}$
No δp_e , no GK ion	1.10×10^{-6}	3.80×10^{-6}	1.12×10^{-5}	1.92×10^{-5}
With δp_e , no GK ion	1.37×10^{-6}	4.47×10^{-6}	1.28×10^{-5}	2.46×10^{-5}
No δp_e , with GK ion	1.10×10^{-6}	4.16×10^{-6}	1.21×10^{-5}	2.17×10^{-5}

larger domain. This will be more difficult with more complete physical models, e.g., with kinetic electrons. We have found that, with fully drift-kinetic electrons, this generalized matching technique is essential for simulating the $n = 1$ tearing modes in present-day tokamaks. This fact is largely determined by the size scaling of the mode growth rate in the collisionless and semi-collisional regime, $\gamma \sim a^{-3.5}$.⁵ For a present-day tokamak, the mode growth rate is very low in comparison with typical drift-wave frequency, and the demand on computational resource is prohibitive. We therefore anticipate that gyrokinetic simulations of the low- n tearing modes will proceed with the generalized matching technique. The external region, in general, should be treated with a computationally efficient fluid electron model, and only in a narrow region around the tearing layer a kinetic electron model is used.

ACKNOWLEDGMENTS

We acknowledge Dr. Guo-Yong Fu, Dr. Scott Kruger, Dr. Steve Jardin, Dr. Carl Sovinec, Dr. C.-S Chang, Dr. Jianying Lang, and Dr. Seung-Hoe Ku for helpful discussions. This work was supported by the U.S. Department of Energy's SciDAC projects "Center for Nonlinear Simulation of Energetic Particles in Burning Plasmas" (DE-FG02-08ER54987), "Center for Edge Physics Simulation" (DE-SC0008801), and "Center for Extended Magnetohydrodynamic Modeling" (DE-FC02-08ER54971). This research used resources of the National Energy Research Scientific Computing Center, which was supported by the Office of Science of the U.S. Department of Energy under Contract No. DE-AC02-05CH11231.

APPENDIX: DISCRETIZATION OF THE POLARIZATION DENSITY

The construction of the matrix $M_{m'm}$ proceeds as follows. Consider any point (r_0, θ_0, ζ_0) . We first set up a set of uniformly spaced 2D Cartesian grids on the local perpendicular plane

$$x_i = -\frac{1}{2}L + i\frac{L}{N}, \quad (\text{A1})$$

$$y_j = -\frac{1}{2}L + j\frac{L}{N}, \quad (\text{A2})$$

for $i, j = 0, 1, 2, \dots, N$. Here, L is a box-size to be chosen later. The unit of length in this Cartesian plane is the local ion Larmor radius. In this Appendix, the notation (x, y) stands

for the Cartesian coordinates in this local perpendicular plane. We temporarily use a Fourier expansion in the perpendicular plane as follows:

$$\phi(x, y) = \sum_{k_x, k_y} \phi_{k_x, k_y} e^{ik_x x + ik_y y}, \quad (\text{A3})$$

for $k_x, k_y = i2\pi/L, -N/2 < i < N/2$. Unlike the usual discrete Fourier transform, ϕ_{k_x, k_y} is computed using all grid points in a symmetrical manner

$$\phi_{k_x, k_y} = \frac{1}{N^2} \sum_i^{N-1} \sum_j^{N-1} \phi_{i+1/2, j+1/2} e^{-ik_x x_{i+1/2} - ik_y y_{j+1/2}}, \quad (\text{A4})$$

with $x_{i+1/2} = (x_i + x_{i+1})/2$, $y_{j+1/2} = (y_j + y_{j+1})/2$ and $\phi_{i+1/2, j+1/2} = (\phi_{i,j} + \phi_{i+1,j} + \phi_{i,j+1} + \phi_{i+1,j+1})/4$. Now at the point (r_0, θ_0, ζ_0) which is the origin in the local Cartesian plane, the general form of n_p in Eq. (5) can be written as a sum over the Fourier components k_x and k_y

$$n_p = -\frac{qn}{T} \sum_{k_x, k_y} \phi_{k_x, k_y} (1 - \Gamma_0(b)), \quad (\text{A5})$$

which, by substituting the expression for ϕ_{k_x, k_y} in Eq. (A3), can be written as

$$n_p = \sum_{i,j} M'_{i,j} \phi_{i,j}, \quad (\text{A6})$$

where M' is an auxiliary matrix of dimension $(N+1) \times (N+1)$. We emphasize that Eq. (A6) is an expression for the ion polarization density at the point (r_0, θ_0, ζ_0) , expressed as a weighted sum of the values of ϕ at the grid points in the 2D plane perpendicular to the local equilibrium magnetic field. The local ion density and temperature at (r_0, θ_0, ζ_0) are to be used when constructing the matrix element of M' corresponding to the point (r_0, θ_0, ζ_0) . The matrix M' is constructed in the simulation, but the explicit form is omitted here. The matrix M in Eq. (14) can be obtained by expressing $\phi_{i,j}$ using the form of Eq. (13). That is, we find the exact location (r, θ, ζ) of the grid point (x_i, y_j) , evaluating $\phi_{i,j}$ with the Fourier representation of Eq. (13), using linear interpolation in the radial direction. The procedure is completely general. In a toroidal magnetic equilibrium, the local perpendicular plane does not in general coincide with the poloidal cross section due to the nonzero poloidal field, and this effect on the polarization density will be captured. In the present case, we do treat the poloidal plane (r, θ) as the local perpendicular plane. If we align the y-axis with the r-direction, then the polar coordinate of the point (x, y) is

$$r = \left(x^2 + (r_0 + y)^2 \right)^{1/2}, \quad \theta = \theta_0 + \tan^{-1} \frac{x}{r_0 + y}. \quad (\text{A7})$$

If the point turns out to be outside of the simulation domain $(r_{\text{in}}, r_{\text{out}})$ then it does not contribute to the matrix M .

The auxiliary box-size L should be chosen so that the scheme is sufficiently accurate for the modes of interest. The accuracy of the scheme can be checked by applying the auxiliary scheme Eq. (A6) on a single Fourier component $\phi(x, y) = e^{ikx}$

with arbitrary wave number k . The result is of the form $n_{\text{disc}}(k) e^{ikx}$, with $n_{\text{disc}} = \sum_{i,j} M'_{i,j} e^{ikx_i}$. The exact result is of course $n_{\text{exac}} = 1 - \Gamma_0(b)$. The Pade approximation, $n_{\text{pade}}(k) = b/(1+b)$, is also commonly used in theoretical studies and simulations.^{3,28}

The relative error plotted in Fig. 1 is defined to be $(n_{\text{disc}} - n_{\text{exac}})/n_{\text{exac}}$, for example. The MHD approximation of $n_p = \frac{m_i n_i}{q B^2} \nabla_{\perp}^2$ is obtained in the limit of small k_{\perp} .

¹R. D. Sydora, *Phys. Plasmas* **8**, 1929 (2001).

²W. Wan, Y. Chen, and S. Parker, *Phys. Plasmas* **12**, 012311 (2005).

³B. N. Rogers, S. Kobayashi, P. Ricci, W. Dorland, J. F. Drake, and T. Tatsuno, *Phys. Plasmas* **14**, 092110 (2007).

⁴H. Doerk, F. Jenko, M. J. Pueschel, and D. R. Hatch, *Phys. Rev. Lett.* **106**, 155003 (2011).

⁵J. F. Drake and Y. C. Lee, *Phys. Fluids* **20**, 1341 (1977).

⁶D. Liu, Q. Zhang, J. McClenaghan, J. Wang, and Z. Lin, *Phys. Plasmas* **21**, 122520 (2014).

⁷H. Cai and G. Fu, *Phys. Plasmas* **19**, 072506 (2012).

⁸Y. Lin, X. Y. Wang, L. Chen, X. Lu, and W. Kong, *Plasma Phys. Controlled Fusion* **53**, 054013 (2011).

⁹R. Numata, G. G. Howes, T. Tatsuno, M. Barnes, and W. Dorland, *J. Comput. Phys.* **229**, 9347 (2010).

¹⁰R. Numata, W. Dorland, G. G. Howes, N. F. Loureiro, B. N. Rogers, and T. Tatsuno, *Phys. Plasmas* **18**, 112106 (2011).

¹¹Z. Lin and L. Chen, *Phys. Plasmas* **8**, 1447 (2001).

¹²D. Liu and L. Chen, *Plasma Phys. Controlled Fusion* **53**, 062002 (2011).

¹³Y. Chen and S. E. Parker, *J. Comput. Phys.* **189**, 463 (2003).

¹⁴A. Mishchenko, A. Konies, R. Kleiber, and M. Cole, *Phys. Plasmas* **21**, 092110 (2014).

¹⁵Y. Chen and S. E. Parker, *J. Comput. Phys.* **220**, 839 (2007).

¹⁶J. Lang, Y. Chen, S. E. Parker, and G.-Y. Fu, *Phys. Plasmas* **16**, 102101 (2009).

¹⁷Y. Chen, T. Munsat, S. E. Parker, W. W. Heidbrink, M. A. V. Zeeland, B. J. Tobias, and C. W. Domier, *Phys. Plasmas* **20**, 012109 (2013).

¹⁸J. Wesson, *Tokamaks* (Oxford Science Publications, 2011).

¹⁹H. P. Furth, J. Killeen, and M. N. Rosenbluth, *Phys. Fluids* **6**, 459 (1963).

²⁰Y. Chen and S. E. Parker, *Phys. Plasmas* **8**, 441 (2001).

²¹W. W. Lee, *Phys. Fluids* **26**, 556 (1983).

²²M. Furukawa, S. Tokuda, and L. J. Zheng, *Phys. Plasmas* **17**, 052502 (2010).

²³S. Janhunen, B. Wang, J. Hesthaven, M. Adams, S.-H. Ku, and C.-S. Chang, *Bull. Am. Phys. Soc.* **59**(15), GP8 (2014).

²⁴R. D. Hazeltine and J. D. Meiss, *Phys. Rep.* **121**, 1 (1985).

²⁵M. Kotschenreuther, G. Rewoldt, and W. Tang, *Comput. Phys. Commun.* **88**, 128 (1995).

²⁶J. Candy and R. Waltz, *J. Comput. Phys.* **186**, 545 (2003).

²⁷A. Mishchenko, A. Konies, and R. Hatzky, *Phys. Plasmas* **12**, 062305 (2005).

²⁸Y. Nishimura, Z. Lin, J. L. V. Lewandowski, and S. Ethier, *J. Comput. Phys.* **214**, 657 (2006).